# Three-dimensional effects in the reduction of turbulence-impingement noise of aerofoils by wavy leading edges

Georgios Bampanis & Michel Roger
Université de Lyon, École Centrale de Lyon, France.

**Summary**

The present work is aimed at investigating experimentally the three-dimensional features of the noise radiated by turbulence impinging on the leading edge of a rectangular aerofoil and its reduction by means of an appropriate wavy design of the leading edge. Turbulence-impingement noise is involved in many engineering applications including aircraft propulsion, air conditioning and ventilation systems, and so on. The wavy leading edge is already recognized as an effective aerofoil noise reduction mean but its effectiveness off the mid-span plane has not been addressed yet in spite of its interest for rotating-blade technologies. A dedicated setup is considered in the present work. The aerofoil is held in grid-generated turbulence at the nozzle of an open-jet wind tunnel, between very narrow end-plates, so that the microphone can be placed off the mid-span plane without suffering from masking by the plates. Experiments are performed with baseline (straight) and wavy leading edges. The effect of radiation angle is discussed and the limitation of far-field measurements is assessed by discussing additional source-localisation results.

**PACS no. 43.28.+h, 43.28.Ra**

## 1. Introduction

Flow-generated sound is a dominant problem in many engineering applications in both domestic and industrial environments. Aerodynamic noise produced by rotating blades in low-speed fans such as those used in aircraft propulsion, air-conditioning and ventilating systems, contributes significantly to the total broadband noise of each installation. The majority of the flow environments in these installations are disturbed by turbulent flows produced by elements installed upstream of the fan such as heat exchangers, protection grids, rotor-stator interaction and so on. Two fundamental mechanisms are considered as dominant contributors to the broadband noise of an aerofoil, namely self-noise and turbulence-impingement noise (TIN). Self-noise includes noises produced by vortex-shedding at blunted trailing-edges, blade-tip vortices, flow separation and trailing-edge scattering of boundary-layer turbulence known as trailing-edge noise (TEN). TIN refers to the direct interaction of oncoming vortices with the leading-edge singularity. Geometrical modifications at the leading edge have been recognized as an effective mechanism to reduce the efficiency of vortex dynamics as a sound generator. Many studies on aerofoils and flat plates with sinusoidal leading-edge cuts have been already carried out both experimentally and numerically, by Clair et al. [1], Gruber [2], Haeri et al. [3], Roger et al. [4], Chaitanya et al. [5,9,10], Narayanan et al. [6,7], Kim et al. [8], Roger & Moreau [11]. Kim et al [8] numerically identified two noise reduction mechanism, the existence of a dominant source-cutoff effect due to the obliqueness of the serrated leading edge and a phase-interference effect between the peaks and hills of the serrations. Chaitanya et al. [9] performed a parametric study on the amplitude $h$ and the wavelength $\lambda$ of the serrations and the turbulence integral length scale $\Lambda$. They suggested the existence of an optimum serration inclination angle $\theta_0 = \tan^{-1}(2h/\Lambda)$ for which half the serration wavelength equals the turbulence integral-scale $\Lambda$ and a coherent excitation by the oncoming vortices occurs. More recently Chaitanya et al. [10] obtained larger turbulence-impingement noise reductions by applying hybrid, double-wavelength serrations.

The limitation of previous experimental studies is that sound radiation is only considered in the mid-span plane of the aerofoils. Yet three-dimensional effects are expected from the aforementioned phase-interference effect. Such effects are involved as rotating-blade noise must be assessed for arbitrary observer locations. This is why the current work is aimed at investigating TIN reduction by leading-edge serrations off the mid-span plane. This investigation is made possible by a dedicated setup installed on a rectangular nozzle. The tested rectangular aerofoil is held between two narrow end plates that prevent significant sound reflection and masking, so that the microphone can be placed at quite large angles from the mid-span plane, giving access to oblique radiation. It is worth noting that the jet-ring interaction experiment described by Roger [12] is an alternative and indirect way of measuring TIN radiation off the mid-span plane. The present work still relies on the rectangular-airfoil configuration; it is dealing with a preliminary investigation of the effect of leading-edge serrations on the oblique radiation of TIN, performed within the scope of the European Marie Skłodowska Curie project SmartAnswer.

## 2. Description of the Experiment

### 2.1 Experimental setup

The measurements were carried out in the low-speed open-jet anechoic wind tunnel of Ecole Centrale de Lyon using the installation of a rectangular nozzle with a vertical exit cross-section of 15cm x 30cm. The contraction ratio of the nozzle is 2:1 from an initial section of 30 cm x 30 cm. The mean flow velocity ranges from 19m/s to 32 m/s. A grid made of flat rods is installed upstream of the nozzle contraction, generating nearly isotropic and homogeneous turbulence. The streamwise turbulence spectrum has been measured with a single hot-wire probe at the position of the leading-edge in absence of the tested aerofoil and successfully fitted with a model von Kármán spectrum. This allows deducing the spectrum for the complementary crosswise velocity component that will be used as input for analytical predictions in a future work. The turbulence integral scale has been found as 9 mm and the turbulent intensity as 4.5%. The aerofoil is held vertically at zero angle of attack in the present work, as illustrated in Figs.1 and 2.

The far field pressure was measured on a portion of sphere described by the spherical coordinates $(R, \theta, \varphi)$ (see Fig.1), with origin at the mid-span leading edge of the baseline aerofoil. $x$ is the horizontal, streamwise/chordwise coordinate and $y$ the coordinate normal to the aerofoil. The azimuthal angle $\theta$ is varied by making the horizontal support of microphones move in the $(x, y)$ plane and the polar angle $\varphi$ is explored along the vertical arc of the support. Six microphones B&K $1/2''$ type 4189 with preamplifiers of type 2671 are distributed on the arc, measuring simultaneously the acoustic pressure at the polar angles ranging from 0° to 75° by steps of 15°. The support is placed on a remote-controlled rotating base and is set to allow variations of the angle $\theta$ from 20° to110° from the streamwise direction by steps of 5°. The radius of the measuring sphere is 1.25m, which ensures far-field conditions for the frequency range of interest.

All acquisitions have been made with a sampling frequency of 51.2 kHz with averaging over 30 blocs, ensuring a bandwidth of 1Hz in the frequency range 0-25.6 kHz. When making spectra sub-tractions, the resolution has been reduced to 16 Hz in order to avoid the large high-frequency scatter due to statistical errors.

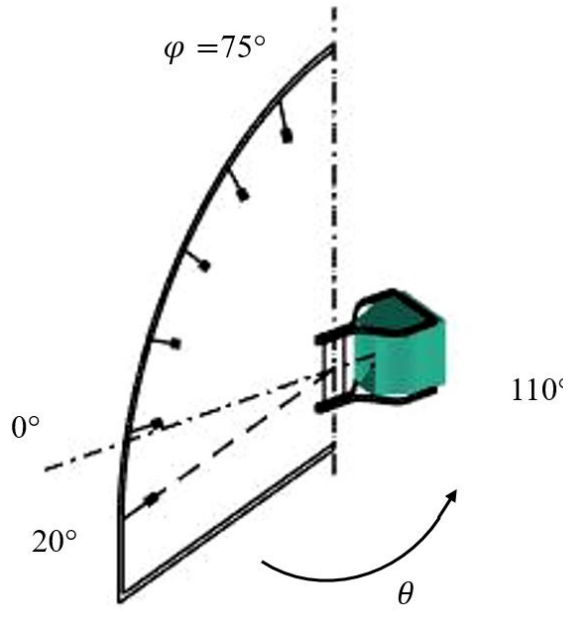


Figure 1. Drawing of the rotating circular microphone array and spherical coordinates.

**EURONOISE 2018**

**28 May - 31 May, Hersonissos**

### 2.2 Mockups manufacturing process

For the sake of quantifying the amount of reduction achieved by serrations, on the one hand, and of comparing to broadband-noise analytical models, on the other hand, a relevant choice of thin baseline aerofoil is needed. Hence, two flat-plate based aerofoils with wavy leading edges and a baseline one with straight edge, used as reference for comparisons, have been manufactured using a three-dimensional printer.

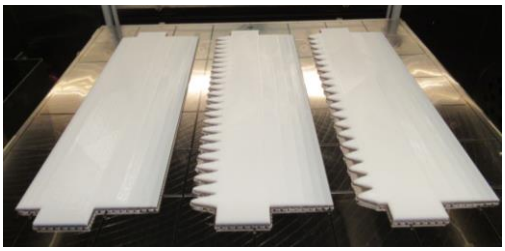

(a)

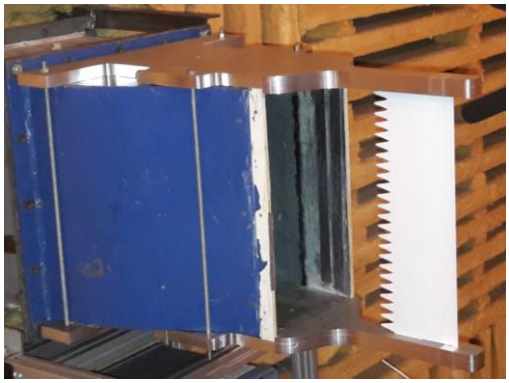

(b)

Figure 2. Experimental installation in the ECL small anechoic wind tunnel: (a) Flat plate mockups, (b) Narrow side plates placed at the exit of the rectangular nozzle.

For the design a standard symmetric NACA-0003 shape has been split into two parts at its maximum thickness point and extended by adding a flat-plate portion in between. This produced aerofoils of 3 mm thickness, $L = 30\,cm$ span and $c = 10\,cm$ mean chord length that have been polished to avoid serration corners and trailing-edge bluntness. The sinusoidal serration profile has been defined around the straight-edge location of the baseline aerofoil, so that all mock-ups have the same area. The parameters of the two serrated versions are defined according to the measured integral length scale $\Lambda$ of the incident turbulence, about 9 mm, accounting for the optimum observed by Chaitanya *et al.* [9]. The expected optimum corresponds to the bigger serrations whereas the smaller serrations are investigated to assess the sensitivity of the results. The parameters are summarized in Table 1.

Table 1. Leading-edge serration parameters (mm)

| Parameter | Large serr. | Small serr. |
|---|---|---|
| $\lambda$ | 12.5 | 15 |
| $h$ | 10 | 7 |

## 3. Noise-Reduction Spectra

The present section highlights the amount of TIN reduction from dB-differences of the far-field sound pressure PSD (power spectral densities) $S_{pp}(f)$ measured with the baseline and serrated aerofoils, including the effect of directivity both in and off the mid-span plane. The Sound Pressure Level (SPL) is defined as

$$\mathrm{SPL}(f) = 10\log\left(S_{pp}(f)/p_{ref}^2\right), \qquad (1)$$

and measured for all $\varphi_i$ angles simultaneously at each $\theta_j$ angle, $p_{ref} = 2.10^{-5}$ being the acoustic reference pressure, in the frequency range between 40 Hz and 14 kHz. Sound spectra are measured both with and without the aerofoil to suppress the contribution of the background noise by simple spectral subtraction. However the noise observed below 40 Hz is attributed to some modification of the background noise sources associated with the free-jet oscillations, which cannot be suppressed by the subtraction procedure. At very high frequencies aerofoil noise decreases below the background

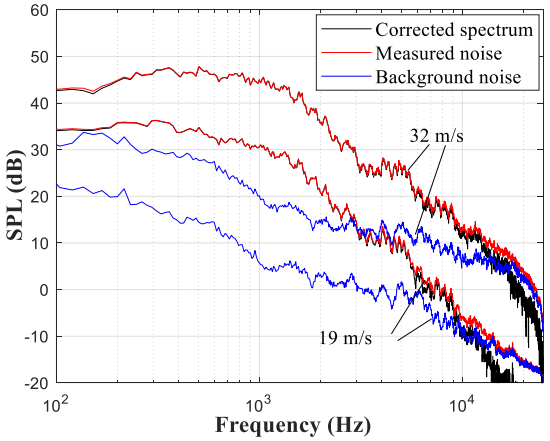


Figure 3. Reference results for the baseline flat plate at angle $\theta = 90°, \varphi = 0°$ for the two mean velocities $U = 19$ and $32\,m/s$. The corrected spectrum (black) is obtained by subtracting the background noise spectrum (blue) from the raw measurement (red).

noise level, no longer allowing further investigation from simple far-field measurements. Self-noise, reduced to trailing-edge noise in the present case, also contributes to the total aerofoil noise at high frequencies, as emphasized later on, which makes the assessment of TIN reduction more questionable. The threshold beyond which TEN takes over TIN will be estimated in the coming months by means of dedicated measurements without turbulence grid. Microphone-array measurements will also be used for the discrimination of sources (see section 5).

### 3.1 Mid-Span Plane Results

A first investigation of the effect of leading-edge serrations in the mid-span plane in a direction normal to the aerofoil is reported in Fig.4. Most of the reduction is achieved between 500 Hz and 10 kHz, with a maximum of about 11 dB in the range 4300-4500 Hz.

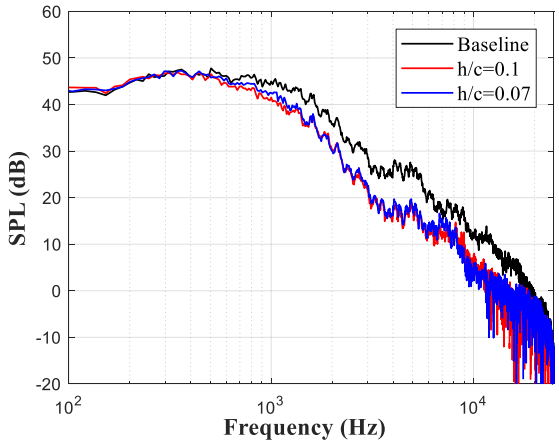


(a)

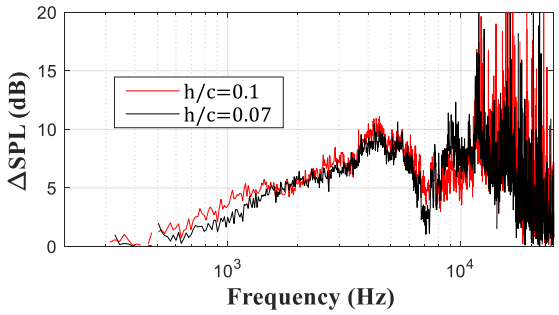


(b)

Figure 4. Far-field sound spectra. (a) All the flat plates at flow speed $U = 32$ m/s at $\theta = 90°, \varphi = 0°$ angles. (b) Noise reduction performances of the serrated flat plates at the same conditions.

The *a priori* optimum serration angle [9] is confirmed by the slightly better performance of the large serrations at low frequencies. Yet Small serrations appear to be more efficient at high frequencies (8-10 kHz), and a dip is found between both regimes. These features will be discussed in the section 5.

### 3.2 Performances Off the Mid-Span Plane

The TIN spectra of the baseline aerofoil measured at $\theta = 90°$ and reported in Fig. 5 show that the sound level decreases as the polar angle $\varphi$ increases from 0° to 75°, according to the dipolar behaviour of the sources (about -12 dB at low frequencies, less at higher frequencies due to non-compactness). TIN reduction by serrations is addressed in this section only for the extreme angles. The corresponding reduction spectra are reported in Figs. 6-(a) and 6-(b) in terms of Strouhal number ($fh/U$) for the flow speeds 27 m/s and 32 m/s, respectively, for the large serrations with $h/c = 0.1$. Though the afore-mentioned two frequency ranges of noise reduction separated by a dip are observed for both values of the $\varphi$ angle, a substantial effect of this angle is observed. The maximum reduction around $fh/U \approx 1.5$ is lower at 75° whereas the reduction is higher at 75° below $fh/U \approx 1$. The poorer reduction off the mid-span plane beyond $fh/U \approx 4$ will be discussed later on from source localisation results.

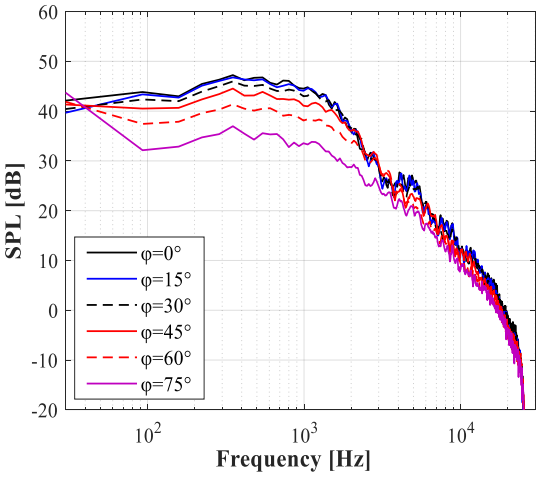


Figure 5. Far-field sound spectra of the baseline for all polar angles $\varphi = 0° - 75°$ at flow speed $U = 32$ m/s.

**EURONOISE 2018**

**28 May - 31 May, Hersonissos**

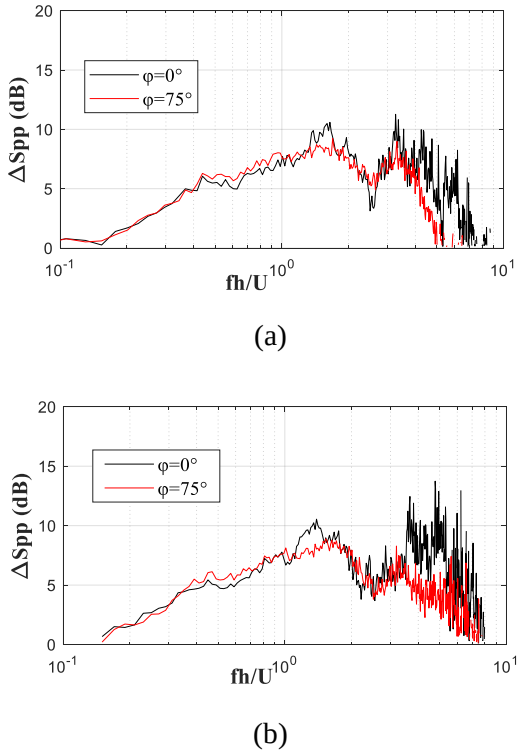


Figure 6. Noise reduction performances of the serrated aerofoil h/c=0.1 for $\varphi = 0°$ and $75°$ at $\theta = 90°$ at different flow speeds (a) $U = 27\ m/s$, (b) $U = 32\ m/s$.

## 4. Directivity results

Directivity patterns of TIN for the baseline and serrated aerofoils with $h/c = 0.1$ are compared in Fig.7 for various polar angles $\varphi$, at both a low frequency of 312 Hz and a high frequency of 4248 Hz corresponding to chord-based Helmholtz numbers $kc$ of 0.58 and 7.85, respectively, and span-based Helmholtz numbers $kL$ of 1.73 and 23.6. The polar plots show clearly the evidence of two general kinds of patterns. The solid line in Fig.7-(a) refers to the mid-span plane at 312 Hz. It nearly coincides with the point-dipole directivity pattern according to $20\log_{10}|\cos\theta|$ and indicates that the aerofoil chord is acoustically compact. In this low-frequency regime the acoustic effects of the wavy leading edge are minor, about 1dB. Because the span is also nearly compact at that frequency, the same directivity is found at 75° with the same global attenuation as that evidenced in Fig.4. In contrast at 4248 Hz, the dipolar behaviour is replaced by a two-lobed pattern in the mid-span plane, as a consequence of chordwise non-compactness. This frequency is close to that of maximum serration-induced reduction but the pattern is the same for both the baseline and serrated aerofoils. When now

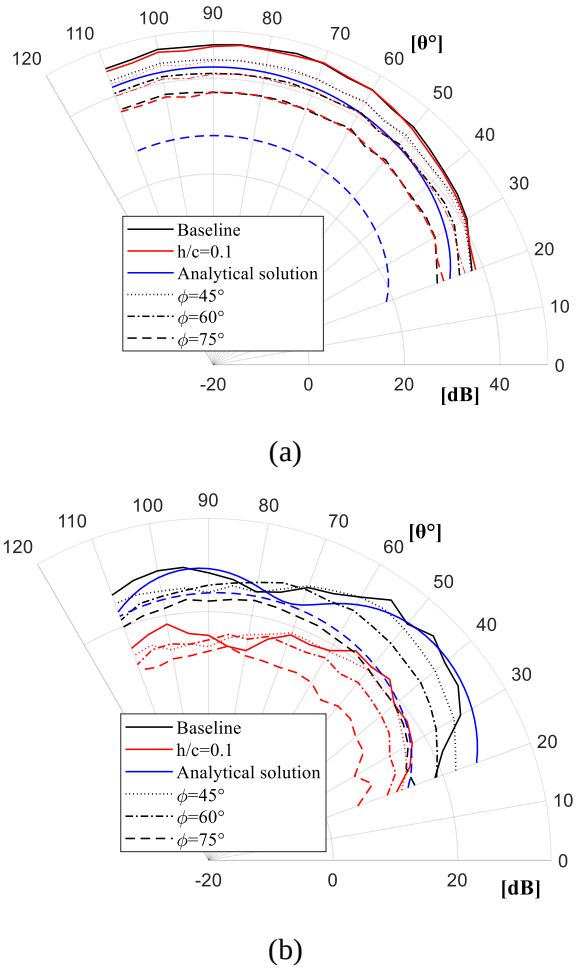


Figure 7. Directivity diagrams for azimuthal angles $\theta = 20° - 110°$ and polar angles $\varphi = 0°$, $\varphi = 45° - 75°$. The blue solid line refers to the analytical solution for the baseline. (a) Directivity patterns at 312 Hz. (b) Directivity patterns at 4248 Hz.

considering the radiation at $\varphi = 75°$ a one-lobed directivity is found again, also for both aerofoils. Despite the differences highlighted in Fig. 6, introducing leading-edge serrations does not modify the basic directivity of the sound. The indicative threshold beyond which the dipolar shape is converted progressively into the two-lobed pattern is around 3.4 kHz (not shown here), corresponding to equal mean chord and acoustic wavelength.

Dealing with the baseline aerofoil only, the measured directivity can be compared to analytical predictions based on Amiet's theory, classically used to model TIN. The theory is not detailed in this paper for the sake of conciseness but a review can be found in references [13,14]. It has been implemented here in its three-dimensional form, fed with the measured turbulent velocity spectrum.

The theoretical directivity diagrams in the mid-span plane and in the same $\theta$ range at $\varphi = 75°$ are also reported in Fig.7 for comparison. Though corrections for the refraction of sound that occurs through the jet shear layers are not accounted for, a very convincing agreement is found at 4028 Hz. The underestimate at 312 Hz is attributed to Amiet's model inaccuracy at low frequencies. This validates the reliability of Amiet's analytical theory as a prediction tool in all directions of space, which to authors' knowledge was not previously addressed. Though not described in the paper, results for intermediate $\varphi$ angles show a progressive change between both extreme values. The lower angles $\varphi = 15°{:}\,30°$ provide results that remain close to those in the mid-span plane, because of the dipolar character of the sources. The change starts being very significant beyond $\varphi = 45°$.

## 5. Source Localization

At high frequencies for which aerofoil noise gets closer to the the background noise or lower, and as TIN is at the same level as TEN, estimating TIN reduction with the subtraction of far-field spectra becomes questionable. TEN can be measured separately by removing the turbulence grid, but this supposes that the boundary layers develop in the same way with and without the grid. If they remain laminar and unstable in a clean flow, self-noise takes the form of tonal noise and additional tripping devices are needed to force the transition to turbulence on the aerofoil. This makes the procedure at least inaccurate. Source identification and localisation by means of microphone arrays then appears as an alternative approach. Several post-processing techniques such as conventional beamforming and advanced coherence techniques can be used. First results are presented in this section based on the CIRA technique recently used at Ecole Centrale de Lyon in other aerofoil noise studies [15].

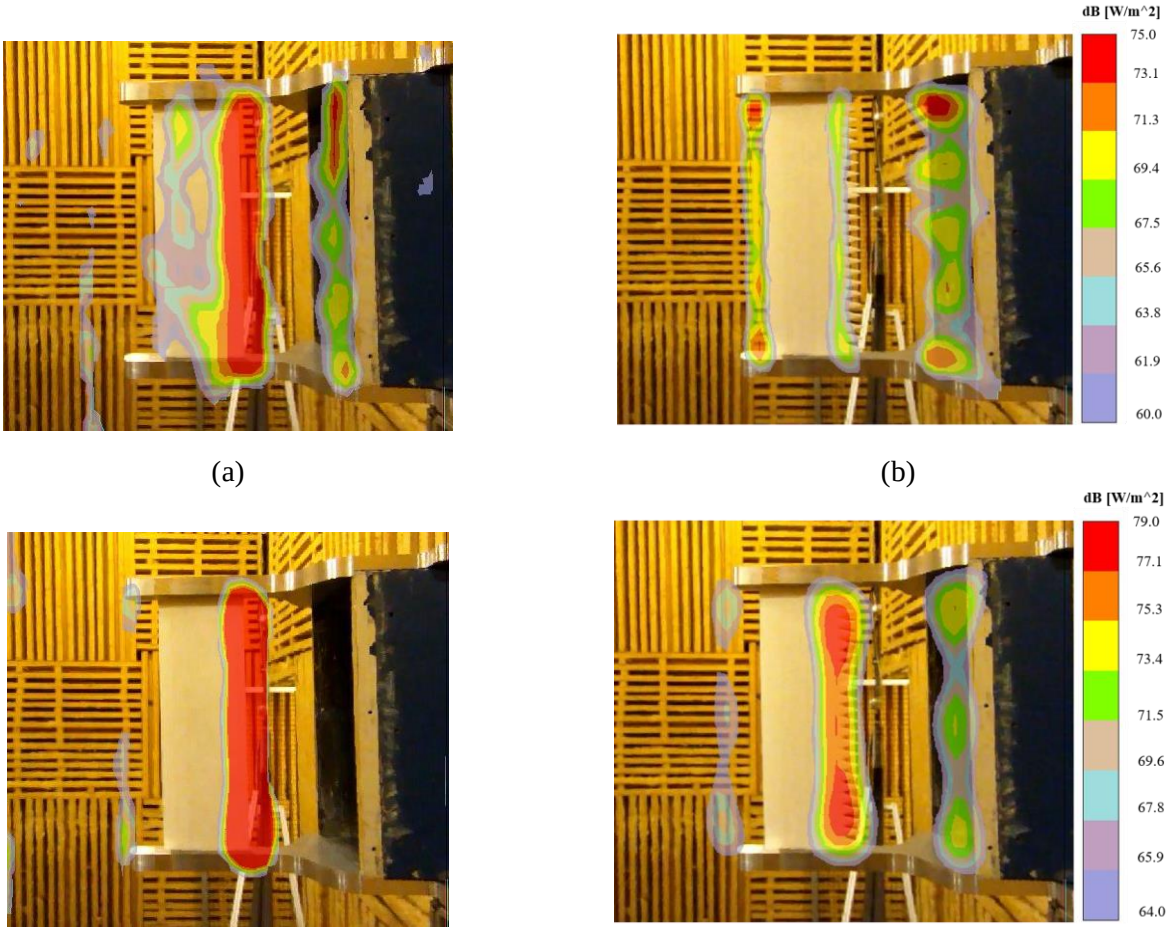


Figure 8. Noise maps for the baseline and serrated aerofoil h/c=0.1 at flow speed U=32 m/s. (a) baseline at 7-7.4 kHz (b) serrated aerofoil at 7-7.4 kHz (c) baseline at 4-4.5 kHz (d) serrated aerofoil at 4-4.5 kHz.

The aim is twofold. In a first step, shortly discussed here, the high-intensity areas of the localisation map are just used to identify the main sources. In a second step, they will be integrated to quantify the multiple sources separately, in order to extract the TIN contribution when it is not emerging in the far-field spectra. This second step will be the matter for future work. A spiral microphone array consisting of 81 sensors placed 0.5 m away from the airfoil and parallel to the flow direction is used in the present study. It is operated by the LMS software provided by MicrodB (Siemens) company. The CIRA algorithm is not described in this section, only adopting the end-user view [15].

Two frequency ranges are selected in Fig.8 for the discussion, namely the range from 7 kHz to 7.4 kHz (Fig.8-(a) & (b)) corresponding to the local minimum of TIN reduction in Fig.4-(b) and the range from 4 kHz to 4.5 kHz (Fig.8-(c) & (d)) corresponding to the maximum reduction. The baseline aerofoil signature is plotted on the left in Fig.8-(a) & (c) and that of the serrated aerofoil on the right in Fig.8-(b) & (d). Two main noise sources are identified apart from the expected TIN source distributed along the leading-edge. One is detected at the nozzle lips; it attributed to the noise generated by the turbulence grid and the trailing-edge noise of the nozzle itself. The other one is the TEN contribution of the aerofoil. At 4-4.5 kHz in Fig.8-(c) & (d), the leading-edge source clearly dominates for both aerofoils. Indeed although the noise reduction is about 9 dB in Fig.8-(d), the dominant source is still along the leading edge. Therefore the subtraction is relevant to estimate the amount of TIN reduction. Using the same dynamic scale, a different conclusion holds around 7-7.4 kHz in Fig.8-(a) & (b). The leading-edge source of the serrated aerofoil is now at the same level as other sources, and even slightly lower. The subtraction from far-field spectra is no longer representative of the TEN reduction. This suggests that all high-frequency results beyond the Strouhal number $fh/U \approx 1$ in Fig.6 are not representative. The next step will be the extraction of the true TIN level from localisation maps such as in Fig.8-(b) for a proper reconstruction of the targeted information.

## 6. Concluding remarks

The present ongoing work extends previous investigations of the reduction of aerofoil turbulence-impingement noise by means of leading-edge serrations, by paying attention to the reduction achieved off the mid-span plane. This is made possible up to an angle of 75° away from this plane on a portion of sphere by using an open-jet wind-tunnel setup of minimum obstruction. The outcomes are summarised below.

- The maximum noise reduction has been found up to 11 dB in the mid-span plane, in a range of Strouhal number based on the serration amplitude around 1.5. Yet the reduction can be larger at 75° than in the mid-span plane at lower frequencies. The reduction observed at much higher frequencies, for Strouhal numbers exceeding 3, can also be attributed to some contamination by trailing-edge noise sources. The reduction spectra exhibit a narrow dip between both ranges of Strouhal numbers.

- A preliminary source localisation with a microphone array has confirmed the high-frequency contamination by trailing-edge noise and background noise sources. The localisation technique will be used in a future work to extract turbulence-impingement noise; this will allow assessing the true benefit of the serrations in the high-frequency limit and explaining the aforementioned dip.

- The directivity patterns of turbulence-impingement noise do not differ fundamentally for straight and serrated leading edges, apart from the modest variations of the amount of reduction with observation angle. This confirms the effectiveness of the technique for rotating-blade technologies.

- By the way the close agreement of analytical Amiet's model with the measurements performed off the mid-span plane with the baseline aerofoil extends the validation of the model for arbitrary radiation directions.

**Acknowledgements**

This study has received funding from the European Union's Horizon 2020 research and innovation programme under the Marie Skłodowska Curie, grant agreement No 722401. It was performed within the framework of the Labex CeLyA of the Université de Lyon, within the programme 'Investissements d'Avenir' (ANR-10-LABX-0060/ANR-11-IDEX-0007) operated by the French National Research Agency (ANR).

## References


[1] V.Clair, C. Polacsek, T. Le Garrec & G. Reboul (2012) - CAA Methodology to simulate turbulence-airfoil noise, 18th AIAA/CEAS Aeroacoustics Conference, paper 2012-2189, Colorado Springs CO.

[2] M. Gruber, Airfoil noise reduction by edge treatments, PhD Dissertation, Faculty of Engineering and the Environment, University of Southampton, 2012.

[3] S. Haeri, J. W. Kim, S. Narayanan, and P. Joseph. 3d calculations of aerofoil-turbulence interaction noise and the effect of wavy leading edges. In 20th AIAA/CEAS Aeroacoustics Conference, number 2014-2325, Atlanta, GA, June 2014.

[4] M. Roger, C. Schram, and L. De Santana, Reduction of airfoil turbulence-impingement noise by means of leading-edge serrations and/or porous materials,19th AIAA/CEAS Aeroacoustics Conference, 27–29 May (AIAA, Berlin, Germany, 2013), pp. 2013–2108.

[5] Chaitanya, P., Narayanan, S., Joseph, S., Vanderwell, C., Turner, J., Kim, J. W., and Ganapathisubramani, B., Broadband noise reduction through leading edge serrations on realistic aerofoils, Proceedings of 21st AIAA/CEAS Aeroacoustics Conference, AIAA Paper 2015-2202, Dallas, USA, June 2015. doi:10.2514/6.2015-2202.

[6] S. Narayanan, P. Joseph, S. Haeri, J. W. Kim, P Chaitanya, and C. Polacsek. Noise reduction studies from the leading edge of serrated at plates. In 20th AIAA/CEAS Aeroacoustics Conference, number 2014-2320, June 2014.

[7] S. Narayanan, P. Chaitanya, S. Haeri, P. Joseph, J. W. Kim, and C. Polacsek. Airfoil noise reductions through leading edge serrations. Physics of Fluids, 27(025109), 2015.

[8] Kim, J. W., Haeri, S., and Joseph, P. F., On the reduction of aerofoil-turbulence interaction noise associated with wavy leading edges, Journal of Fluid Mechanics, Vol. 792, 2016, pp. 526{552. doi:10.1017/jfm.2016.95.

[9] Chaitanya, P., Narayanan, S., P., J., and Kim, W., Leading edge serration geometries for significantly enhanced leading edge noise reductions, Proceedings of 22nd AIAA/CEAS Aeroacoustics Conference, AIAA Paper 2016-2736 , Lyon, France, June 2016. doi:10.2514/6.2016-2736.

[10] Chaitanya, P., P. Joseph, S. Narayanan, C. Vanderwel, J. Turner, J. W. Kim, and aerofoil B. Ganapathisubramani. Performance and Mechanism of Sinusoidal Leading Edge Serrations for the Reduction of Turbulence–aerofoil Interaction Noise. Journal of Fluid Mechanics 818 (May 2017): 435–64. https://doi.org/10.1017/jfm.2017.141.

[11] M. Roger & S. Moreau, Airfoil Turbulence-Impingement Noise Reduction by Porosity or Wavy Leading-Edge Cut: Experimental Investigations, InterNoise 2016, Hambourg

[12] M. Roger - On broadband jet-ring interaction noise and aerofoil turbulence-interaction noise predictions, J. Fluid Mech. Vol. 653, pp. 337-364, 2010

[13] M. Roger & S. Moreau, Extensions and limitations of analytical airfoil broadband noise models, Int. J. of Aeroacoustics, vol. **9(3)**, pp.273-305, 2010.

[14] M. Roger, Broadband noise from lifting surfaces, analytical modeling and experimental validation. In: Noise sources in turbulent shear flows: fundamentals and applications, CISM series 545, edited by R. Camussi, Springer, p. 289-344, 2013.

[15] G. Yakhina, M. Roger, A. Finez, S. Moreau & J. Giez, Broadband Airfoil-Noise Source localization by Microphone Arrays and Modeling of a Swept Free-Tip Blade, to be presented at the AIAA/CEAS Aeroacoustics Conf. Atlanta, 2018.